Exploiting the polypharmacology of alectinib for synergistic RNA splicing disruption with RBM39 degraders

Authors: Yurui Ma[1], Evon Poon[2], Chenchen Jin[1], Barbara Martins da Costa[2], Yuewei Xu[1,3], Sadiya Quazi[1], Nikolaos Zourdoumis[1], Chiharu Wickremesinghe[1], Louis Chesler[2], Hector C Keun[1]*, Anke Nijhuis[1]*¥

Affiliations:

[1]Department of Surgery & Cancer, Imperial College London; London, UK.

[2]Division of Clinical Studies, The Institute of Cancer Research, London, UK

[3]Wisdom Lake Academy of Pharmacy, Xi'an Jiaotong-Liverpool University, Suzhou 215123, China (current affiliation)

***Co-corresponding author**

¥**Lead contact:** Dr Anke Nijhuis

Address: Division of Cancer, Imperial College London, London, UK, W12 0NN.

Email: a.nijhuis@imperial.ac.uk **Phone**: +44 (0) 20 7594 3161

Abstract: Precise control of pre-mRNA splicing is critical for transcriptome integrity, and its disruption is increasingly recognised as a vulnerability in cancer. Here, we identify a functional interplay between two key splicing regulators, RBM39 and serine/arginine protein kinase 1 (SRPK1), and show that dual targeting of these factors severely compromises splicing fidelity in high-risk neuroblastoma. We use the molecular glue indisulam to degrade RBM39 and repurpose the clinical ALK inhibitor alectinib which potently inhibits SRPK1. Co-treatment with indisulam and alectinib inhibited cell proliferation, induced apoptosis, and caused G2/M arrest in multiple cancer cell lines, including *MYCN*-amplified neuroblastoma. RNA sequencing revealed enhanced splicing defects preferentially in DNA repair and genome maintenance related genes following combination treatment, leading to R-loop accumulation and increased DNA damage. In the Th-MYCN/ALK^{F1174L} neuroblastoma mouse model, combination therapy induced complete tumour regression and significantly improved survival rates compared with monotherapies. These findings demonstrate that combining indisulam and alectinib is a promising approach to treat aggressive malignancies such as high-risk neuroblastoma, exploiting the previously untapped polypharmacology of alectinib as a clinical RNA splicing inhibitor and supporting the therapeutic value of co-targeting interdependent splicing factors for synergistic benefit.

INTRODUCTION

The splicing of precursor messenger RNAs (pre-mRNAs) is a critical regulatory step in gene expression, during which non-coding introns are excised to produce functional mRNA(1). This process is tightly controlled by splicing factors, governing the recognition and selection of splice sites, thereby generating mRNAs with varying exon combinations and consequently diverse protein isoforms(1). Dysregulated alternative splicing can promote tumorigenesis and chemoresistance. Aryl sulfonamides such as indisulam have emerged as promising anticancer agents by targeting an RNA splicing factor RBM39 (RNA binding motif 39)(2,3). These molecular glues facilitate the association of RBM39 with the CUL4-DCAF15 ubiquitin ligase, resulting in RBM39 polyubiquitination and subsequent proteasomal degradation(2,4). Suppressing RBM39 efficiently inhibits tumour growth and advancement through modulating the transcription of various genes associated with tumorigenesis (reviewed in (3)).

One cancer type particularly vulnerable to splicing perturbation is neuroblastoma(5), a common and aggressive extracranial solid tumour in young children, and a major contributor to paediatric cancer mortality(6). High-risk neuroblastoma, comprising approximately 15% of all neuroblastoma cases, represents a distinct subtype characterized by aggressive tumour behaviour and an unfavourable prognosis(7). One pivotal factor contributing to the progression of high-risk neuroblastoma is the amplification of the MYC family transcription factor, MYCN, which can block the differentiation of neural progenitors, the key event in neuroblastoma initiation(8), and plays a crucial role in facilitating the transcriptional repression of tumour suppressor genes(6,7). Furthermore, oncogenic gain-of-function mutations in the *ALK* (Anaplastic Lymphoma Kinase) occur in 10–15% of primary tumours, making ALK the most common single-gene alteration in

57 high-risk neuroblastoma for which targeted clinical therapies have been developed(6,9) Alectinib,
58 an FDA-approved ATP-competitive ALK tyrosine kinase inhibitor (TKI),was initially developed
59 for non-small-cell lung cancer and has shown considerable promise in addressing neuroblastoma
60 in extensive preclinical studies(10-12). However, tumour heterogeneity and resistance to treatment
61 with ALK inhibitors (and molecularly-targeted drugs in general) limit their efficacy as
62 monotherapies(13). Thus, novel strategies, particularly combination therapies, remain important
63 as a means to reduce the toxicity of any single drug and overcome treatment resistance more
64 efficiently. This approach is particularly advantageous in childhood cancer, where long-term
65 toxicity is a major lifelong issue (14).
66
67 Our previous study(15) and others(16) have recognized the exquisite sensitivity of high-risk
68 neuroblastoma to indisulam, with complete responses observed in multiple xenografts, patient-
69 derived xenografts (PDX) and transgenic mouse models. Notably, cells with MYCN amplification
70 exhibit increased sensitivity to aryl sulfonamides, potentially due to their enhanced dependence on
71 RNA processing machinery driven by elevated N-Myc/c-Myc activity, rendering them more
72 susceptible to RNA splicing interference (17). Through the induction of splicing errors in genes
73 within key oncogenic pathways, indisulam can render cancer cells susceptible to additional
74 disruptions caused by other anticancer drugs. For example, we previously showed that several
75 DNA damage repair (DDR) genes are mis-spliced following RBM39 depletion, increasing
76 sensitivity to PARP inhibitors in ovarian high-grade serous carcinoma(18).
77
78 In this study, we sought to further define combinatorial vulnerabilities arising from spliceosome
79 disruption through drug-drug library screens combining indisulam with FDA approved anti-cancer

agents across various cancer models. This approach revealed a synergistic interaction between indisulam and ALK-inhibitor alectinib, likely due to activity against a recently discovered secondary target of alectinib, RNA Serine-Arginine Protein Kinase 1 (SRPK1) (19). SRPK1 promotes the nuclear translocation and activation of a family of SR splicing factors (SRSFs). The combination of indisulam and alectinib simultaneously depletes RBM39 and inhibits SRPK1-mediated SRSF phosphorylation, resulting in exacerbated RNA splicing defects. The subsequent failure to resolve accumulated DNA damage and R loops results in cell cycle arrest, cell growth inhibition and apoptosis of neuroblastoma cells *in-vitro* and tumour regression *in vivo*. Our study provides important proof-of-concept evidence for the co-targeting of splicing factors as a viable strategy to treat aggressive malignancies such as MYCN-driven high-risk neuroblastoma.

RESULTS

Combination drug screens revealed synergy between indisulam and alectinib.

We previously demonstrated that indisulam-mediated RBM39 degradation causes wide-spread RNA splicing defects, and an enrichment in aberrant expression of proteins that mediate DNA damage repair and cell cycle regulation, across various cancer types(15,18,20). This led us to speculate that indisulam is likely to generate drug-induced-vulnerabilities that potentiate the efficacy of existing, clinically approved anti-cancer compounds, such as PARP inhibitors(18). RBM39 degraders, such as indisulam and E7820, have been trialed in 47 clinical studies(3), highlighting potential therapeutic combinations ready for clinical evaluation.

To explore this concept, we conducted two drug-library screens combining indisulam with 147 FDA-approved anticancer drugs (NCI plate number #4891, #4892) in an indisulam-sensitive cell

line (HCT116, colorectal cancer) and an indisulam-resistant line (KURAMOCHI, ovarian cancer). Drugs were tested at 5 doses (16 nM to 10 μM) and combined with DMSO or indisulam at fixed doses (GI30=50 nM for HCT116, 10 μM for KURAMOCHI) (**Fig. 1a, Supplementary Fig.1a**). Bliss scores(21) were calculated to identify synergistic interactions with indisulam. Depletion of RBM39 by indisulam is dependent on DCAF15 expression, thus we generated CRISPR-Cas9 knockouts of *DCAF15* to identify RBM39-specific drug-drug interactions (HCT116 *DCAF15* wild-type (*DCAF15*^{WT}) clone #1 and #2 and *DCAF15* knock-out clones (*DCAF15*^{KO}) clone #1 and #2). Drugs with Bliss score>0 in both HCT116-*DCAF15*^{WT} clones were selected as hits which were further validated in triplicate experiments with selected doses in both HCT116-*DCAF15*^{WT} and *DCAF15*^{KO} clones #1 and #2 and ranked by mean Bliss scores of both cell lines. Most of the synergistic drug-drug interactions were rescued in HCT116-*DCAF15*^{KO} cells suggesting that the synergy is dependent on *DCAF15* and RBM39 degradation (**Fig. 1b left**). In KURAMOCHI, the top 20 hits were ranked by mean Bliss scores across all doses (**Fig. 1b right**). The clinical ALK inhibitor alectinib demonstrated strong synergy in both HCT116 (top hit) and KURAMOCHI (second hit) and was therefore selected for further validation using a wider range of drug concentrations. Strong synergistic growth inhibition was observed across a range of doses of indisulam and alectinib in HCT116 (**Fig. 1c**) and KURAMOCHI (**Fig. 1d**), and the synergy was abrogated in HCT116-*DCAF15*^{KO} cells.

These data confirm that combining alectinib with RBM39 degraders yields synergistic growth inhibition, supporting a potential combination therapy across diverse cancer types.

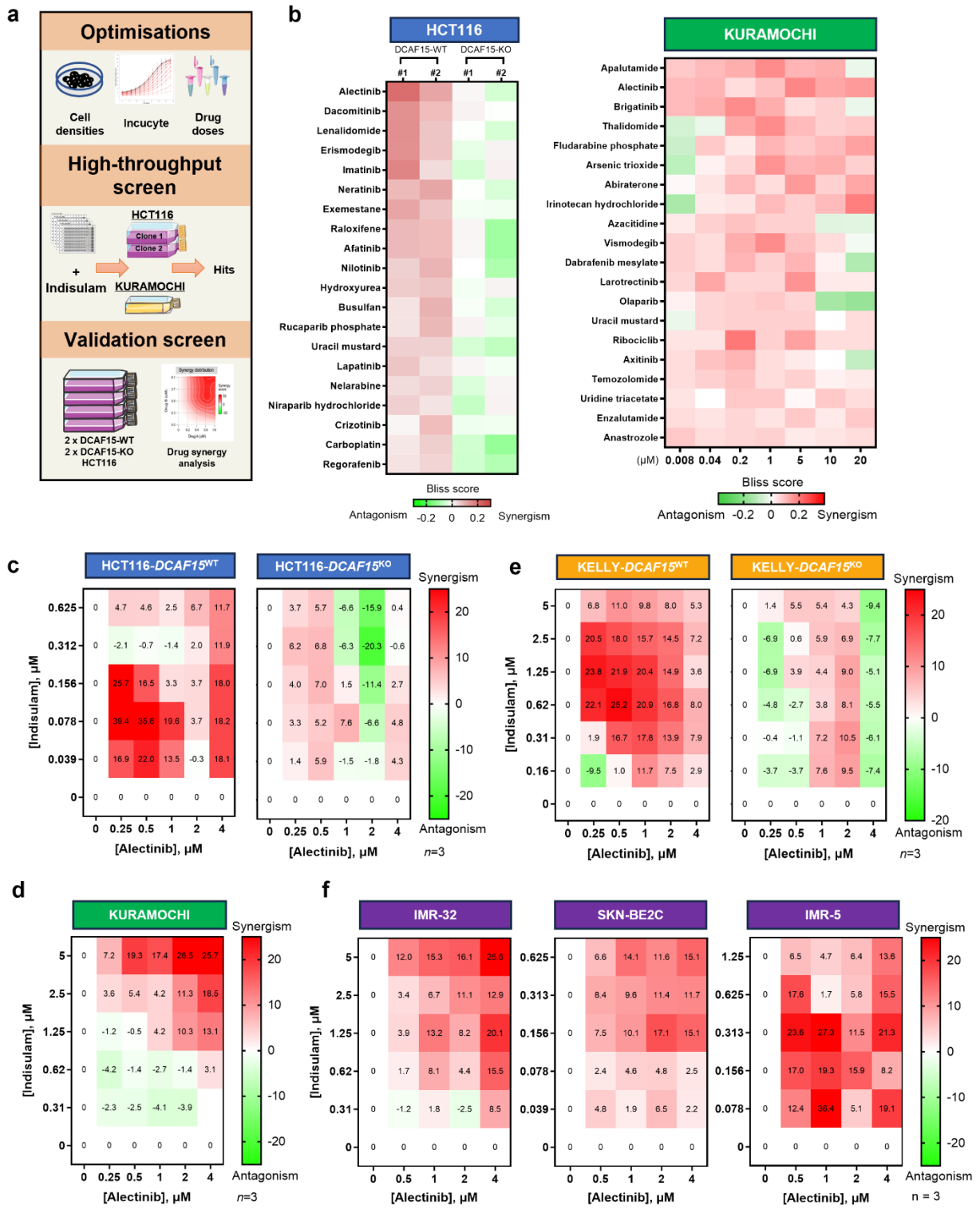

Figure 1. Combination drug screens revealed a synergistic growth inhibition of indisulam and alectinib. a Workflow of combination drug screens in HCT116 and KURAMOCHI using

127 indisulam and 147 FDA-approved anticancer compounds. b Top 20 hits from drug screens in
128 HCT116 (left) and KURAMOCHI (right). HCT116-*DCAF15*^{WT} or HCT116-*DCAF15*^{KO} were
129 treated with selected hits ± indisulam. Bliss scores were calculated from SRB assay data; >0 (red)
130 indicates synergy. KURAMOCHI cells were treated similarly. n=3.; Top 20 hits are ranked by
131 mean bliss score. n=3 replicates. **c-f** Cell lines used for synergy screen (**c, d**) and indicated HRNB
132 cell lines (**e, f**) were treated with alectinib combining indisulam for 72 hours and analysed for cell
133 growth by SRB. Synergy scores were calculated by Synergyfinder (https://synergyfinder.fimm.fi/)
134 using the Loewe method.

135

136 **Indisulam and alectinib exhibit synergistic anticancer efficacy in high-risk neuroblastoma**

137 Considering the potency demonstrated by both indisulam and alectinib as monotherapies in high-
138 risk neuroblastoma(11,15), we further investigated the combination of indisulam and alectinib in
139 four high-risk neuroblastoma cell lines (KELLY, IMR32, SKNBE2C, IMR5) (**Fig. 1e-f**). We
140 demonstrate that combining alectinib with indisulam significantly inhibits cell proliferation
141 compared to monotherapies and display great synergy across a wide-range doses of both
142 compounds on neuroblastoma cell lines, but only additive or antagonistic effects were found in
143 KELLY-*DCAF15*^{KO} cell line confirming the necessity of RBM39 degradation for this
144 pharmacological interaction (**Fig. 1e right**). Similar synergy profiles were observed between
145 alectinib and E7820, a second aryl sulfonamide RBM39 degrader (2)(**Supplementary Fig.1b-c**).

146

147 In addition, alectinib treatment alone did not induce cell apoptosis, but significantly increased the
148 percentage of apoptotic cells when combined with indisulam in KELLY and IMR32 (**Fig. 2a-b,**
149 **Supplementary Fig.2d**). Correspondingly, a significant increase of cleaved caspase 3 was

150 detected in the combination treatment group in KELLY cells (**Fig. 2c**). To evaluate cell cycle
151 progression, we used flow cytometry analysis and detected a notable accumulation of cells in the
152 G2/M phases following 48-hour treatment of indisulam which is consistent with a previous
153 study(16). Co-treatment with indisulam and alectinib increased the percentage of cells in the G1-
154 phase, implying enhanced cell cycle arrest in both G2/M and G1 phase, with a substantial decrease
155 in the percentage of cells in S-phase (**Fig. 2d-e**). These data confirm that indisulam and alectinib
156 act synergistically to suppress the proliferation of neuroblastoma cells, disrupt cell cycle and
157 induce cell apoptosis.
158

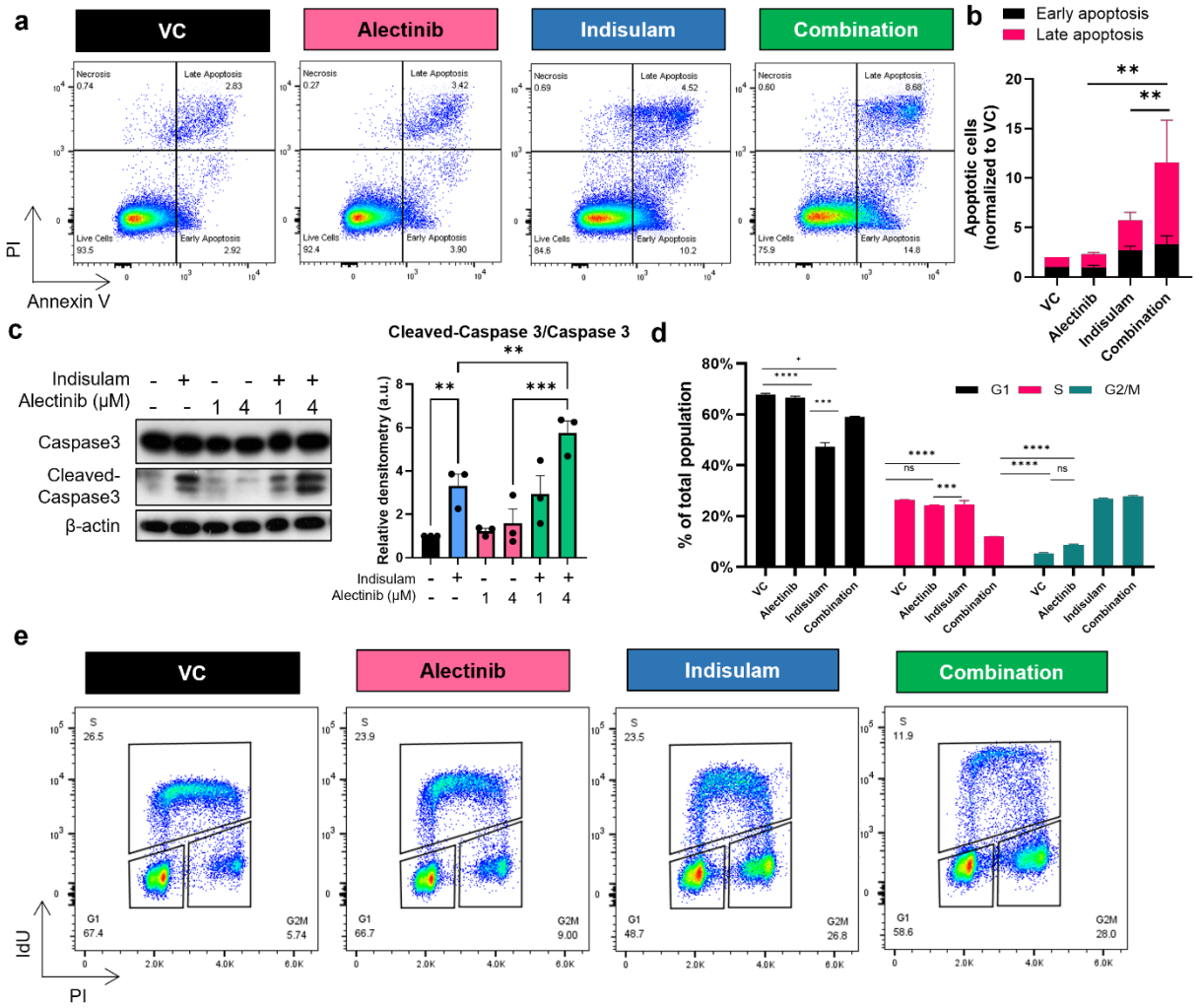

Figure 2. Indisulam and alectinib induce apoptosis and cell cycle disruption in high-risk neuroblastoma. a-b Apoptosis analysis via flow cytometry in KELLY cells after 48h treatment with 1.25μM indisulam, 4μM alectinib, or their combination. Cells were labelled by Annexin V and propidium iodide (PI). The significance of difference of total apoptotic cells was calculated by one-way ANOVA. **c** Western blot of KELLY cells treated with indicated doses of indisulam and alectinib for 48 hours. (n=3 independent experiments) significance of difference was calculated by one-way ANOVA. **d-e** Cell cycle analysis by flow cytometry after 48 h treatment with indisulam, Alectinib, or the combination. Cellular DNA content was labelled with PI, replicating cells were labelled with nucleotide analogues 5-Iodo-2-deoxyuridine (IdU). n=3 independent experiments.

169 Two-way ANOVA were employed to determine the statistical significance among the groups. n.s.
170 not significant, * $p < 0.05$, **$p<0.01$, ***$p < 0.001$, ****$p < 0.0001$.
171

172 **ALK inhibition by alectinib is not required for synergistic interaction with indisulam.**

173 According to data from the Human Protein Atlas (proteinatlas.org) (22) ALK and RET, both
174 primary targets of alectinib, are expressed in NB cells but not in HCT116 and KURAMOCHI (**Fig.**
175 **3a, Supplementary Table 1**) in which synergy was initially discovered. Western blotting
176 confirmed an absence of ALK expression in these cells (**Fig. 3b**). To further test whether the
177 synergy is driven by ALK inhibition, we transfected KELLY, HCT116, and KURAMOCHI cells
178 with an siRNA targeting ALK (siALK) prior to indisulam dosing (**Fig. 3b**). We found no
179 significant difference in cell growth inhibition between siALK and non-targeting control (siNTC)
180 transfected cells (**Fig. 3c**), indicating that ALK inhibition alone does not increase sensitivity to
181 indisulam. We also tested a second ALK inhibitor with a distinct chemical scaffold and binding
182 site, lorlatinib, and found that this compound did not enhance sensitivity to indisulam, except in
183 KELLY cells, which express a mutant, oncogenic form of ALK (ALK^{F1174L}) (**Fig. 3d and**
184 **Supplementary Fig.2a**). However, in cell lines with wild type ALK (IMR32) or lacking ALK
185 expression (HCT116 and KURAMOCHI) there was no sensitization (**Fig. 3d**), consistent with
186 other studies (23), indicating that the efficacy of lorlatinib is specific to ALK mutated
187 neuroblastoma. Further experimental validation is needed to clarify the interaction between
188 inhibition of mutant ALK-driven tumours and RBM39 depletion by indisulam. Nonetheless, these
189 findings suggest that ALK inhibition is not a significant contributor to the synergy we observe
190 between alectinib and the RBM39 degraders indisulam and E7820. This suggests that synergy with
191 RBM39 degradation relates primarily to inhibition of a secondary target of alectinib.

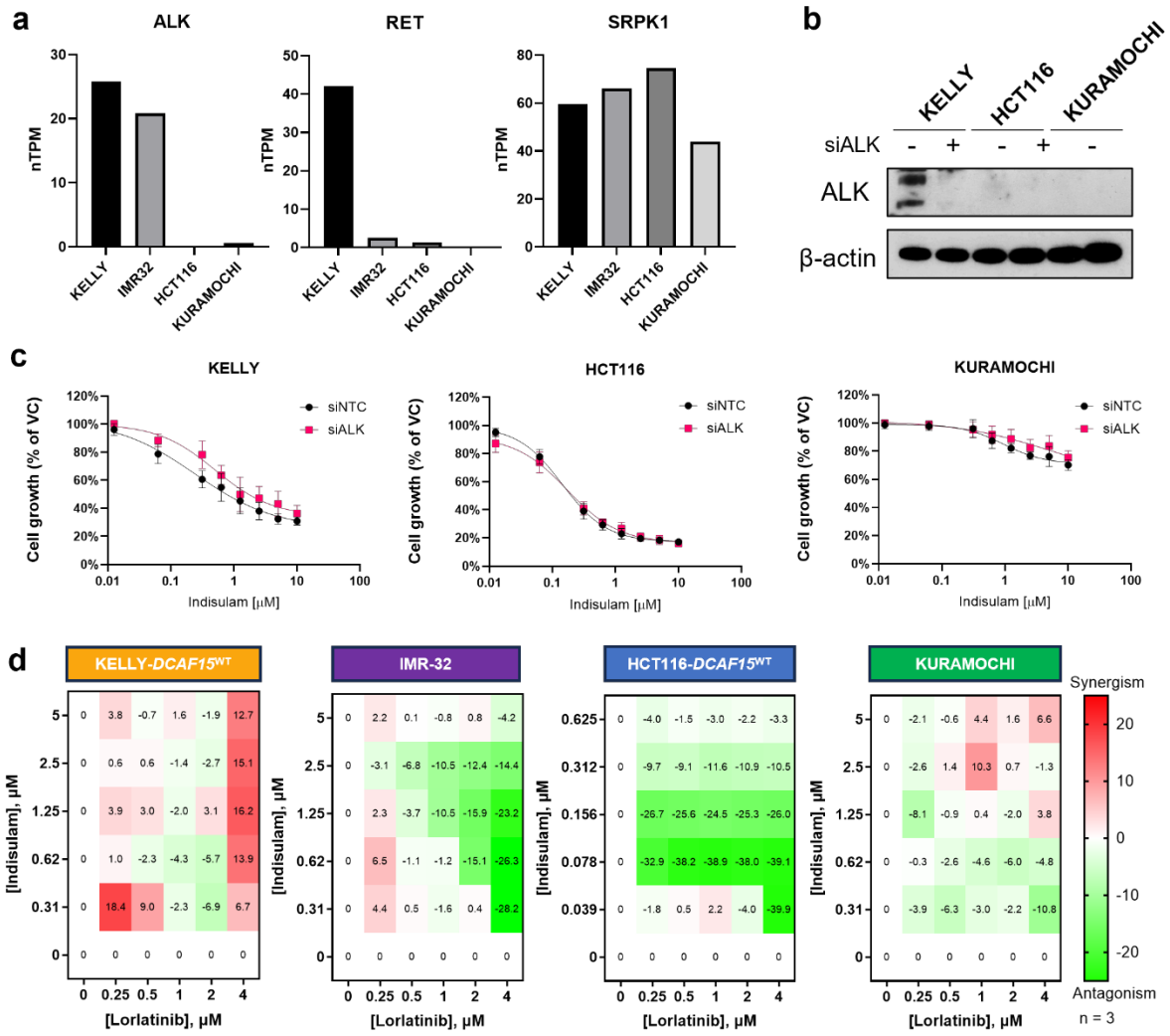

Figure 3. ALK inhibition by alectinib is not an essential determinant of indisulam synergy. a RNA expression data as normalized transcript per million (nTPM) values of cancer cell lines were obtained from proteinatlas.org. **b** Western blot confirming the knock-down of ALK gene expression in cells post transfection with siNTC or siALK. **c** Indicated cell lines were transfected with siALK or siNTC for 16 hours, followed by exposure to indisulam for 72 hours. Cell growth was measured by SRB assay. **d** Indicated cell lines were treated with lorlatinib and indisulam concentration matrix for 72 hours. Loewe synergy scores are plotted. n=3 replicates.

Alectinib exerts potent inhibition of SRPK1.

202 Comprehensive kinase inhibitor screens indicate that alectinib inhibits an array of additional
203 kinases other than ALK (19). The observation that alectinib is a potent inhibition of Serine/arginine
204 (SR) Protein Kinase 1/2 (SRPK1/2) (19,24) is particularly relevant to our research of aberrant
205 RNA splicing. Both SRPK1 and 2 play a central role in regulation of alternative splicing via
206 phosphorylation and activation and nuclear translocation of the Serine/Arginine-rich Splicing
207 Factors (SRSFs) (25,26). In MYCN-amplified neuroblastoma, SRPK1 expression is elevated and
208 associated with reduced survival rates (**Supplementary Fig.2b-c**). In contrast, lower survival rates
209 are not associated with increased expression of SRPK2 nor SRPK3, indicating an increased
210 dependency on SRPK1 to drive tumour growth in MYCN-amplified tumours. Furthermore, a
211 genome-wide CRISPR study showed that loss of SRPK1 sensitizes to indisulam treatment in
212 various solid tumour cell lines (27). Thus, we further explored the treatment combination of
213 SRPK1i and RBM39 degraders. To this end, we assessed the synergy between indisulam and
214 SPHINX31, a known SRPK1 inhibitor(28). Co-treatment of SPHINX31 and indisulam exhibited
215 synergistic growth inhibition cancer across all three cell lines (**Fig. 4a**). Time-lapse cell confluency
216 monitoring in KELLY-*DCAF15*^{WT} and *DCAF15*^{KO} showed that co-treatment significantly
217 suppressed the growth of KELLY-*DCAF15*^{WT}, compared to individual drug treatments.
218 Conversely, in the absence of *DCAF15*, the combination therapy displayed similar potency to
219 SPHINX31 monotherapy (**Fig. 4a**), suggesting this interaction is DCAF15-dependent and thus
220 RBM39-dependent.
221
222 The inhibition of SRPK1 by alectinib was confirmed by enzyme activity assays which reported a
223 half-maximal inhibitory concentration (IC50) of 26nM. This inhibition is more potent than that of
224 SPHINX31 (IC50 = 375nM) with lorlatinib showing very little inhibitory action (**Fig. 4c**).

225 Comparison of the crystal structures of the SRPK1-Alectinib and SRPK1-SPHINX31 complexes
226 confirmed that alectinib and SPHINX31 interact with the ATP-binding groove of SRPK1, with
227 reasonable affinity and occupying similar positions within the binding site (**Fig. 4d** and
228 **Supplementary Fig.3**). Notably, alectinib inhibited SRPK2 with an IC50 of 700nM while
229 SPHINX31 showed no inhibitory effect (**Supplementary Fig.2d**).
230
231 SRPK1 phosphorylates SRSFs, triggering their nuclear translocation and activity in modulating
232 RNA splicing (**Fig. 4e**). Both alectinib and SPHINX31 reduced phosphorylated SRSF (p-SRSF)
233 in KELLY, HCT116 and KURAMOCHI cells (**Fig. 4f)** and decreased the nuclear-to-cytoplasmic
234 ratio of p-SRSF intensity within 4 hours in KELLY cells, while lorlatinib lacked this effect (**Fig.**
235 **4g**). SRSFs are known to promote selection of the proximal splice site in *VEGF* pre-mRNA and
236 inhibiting SRPK1 alters *VEGF* splicing to generate the *VEGF165b* isoform(19,29). Treatment of
237 both alectinib and SPHINX31 resulted in a switch and increased *VEGF165b* mRNA in high-risk
238 neuroblastoma cells (**Fig. 4h**).
239
240 In conclusion, our findings reveal that alectinib is a potent inhibitor of SRPK1, consequently
241 modulating downstream function and RNA splicing through a reduction in the phosphorylation of
242 SRSF splicing factors. Notably, alectinib demonstrates more robust inhibition of SRPK1 as
243 compared to the selective inhibitor SPHINX31, an intriguing observation that could potentially
244 expedite the clinical repurposing of alectinib as an SRPK1 inhibitor.

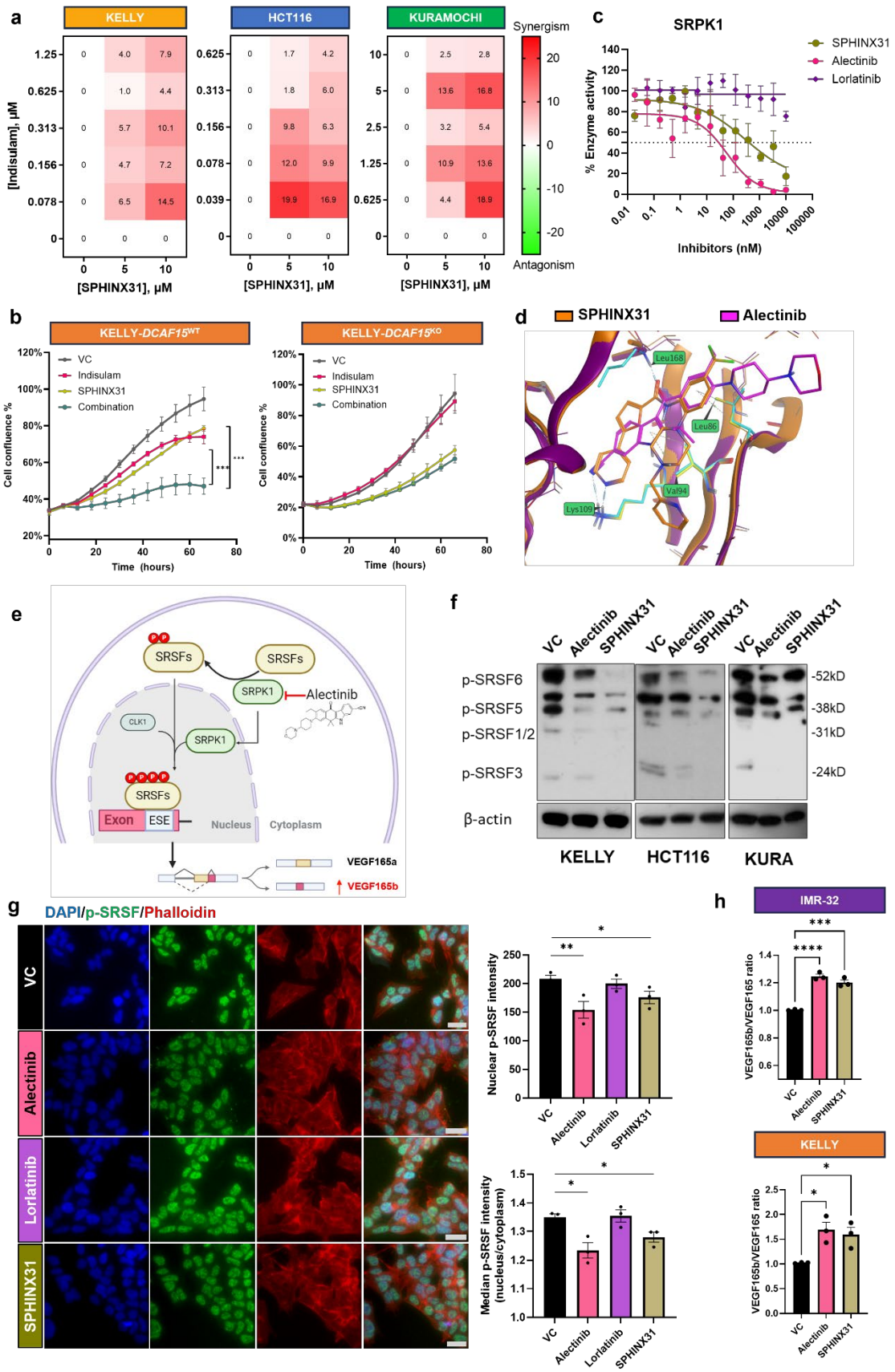
a
KELLY
HCT116
KURAMOCHI
[Indisulam], μM
[SPHINX31], μM
Synergism
Antagonism
c
SRPK1
SPHINX31
Alectinib
Lorlatinib
% Enzyme activity
Inhibitors (nM)
b
KELLY-DCAF15WT
KELLY-DCAF15KO
VC
Indisulam
SPHINX31
Combination
Cell confluence %
Time (hours)
d
SPHINX31
Alectinib
Leu168
Leu86
Val94
Lys109
e
SRSFs
SRPK1
Alectinib
CLK1
Exon
ESE
Nucleus
Cytoplasm
VEGF165a
VEGF165b
f
VC
Alectinib
SPHINX31
p-SRSF6
p-SRSF5
p-SRSF1/2
p-SRSF3
β-actin
-52kD
-38kD
-31kD
-24kD
KELLY
HCT116
KURA
g
DAPI/p-SRSF/Phalloidin
VC
Alectinib
Lorlatinib
SPHINX31
Nuclear p-SRSF intensity
Median p-SRSF intensity (nucleus/cytoplasm)
h
IMR-32
KELLY
VEGF165b/VEGF165 ratio

246 **Figure 4. SRPK1 inhibition is synergistic with indisulam in high-risk neuroblastoma. a**
247 Indicated cell lines were treated with indisulam and SPHINX31. Loewe synergy scores as
248 indicated. **b** KELLY-*DCAF15*^{WT} and *DCAF15*^{KO} cells were treated with indisulam and SPHINX31
249 individually or in combination for 72 hours. Cell confluence was monitored every 6 hours using
250 the Incucyte live cell imaging system. One-way ANOVA was used to determine significance. **c**
251 SRPK1 enzyme activity measured with ADP-Glo™ Kinase Assay with indicated doses of
252 compounds. **d** Alectinib (pink) docked into SRPK1 complexed with SPHINX31(orange). **e**
253 Diagram depicting Alectinib inhibition against SRPK1. Made with Biorender. **f** Western blotting
254 of p-SRSF in KELLY, HCT116 and KURAMOCHI post-treatment. **g** Immunofluorescent staining
255 of p-SRSF in KELLY post-treatment. Nuclear intensity and cytoplasmic staining intensity are
256 calculated using DAPI and Phalloidin (F-actin) segmentation. Scale bar = 20µm. **h** qRT-PCR of
257 *VEGF165b* and total *VEGF165* in KELLY and IMR32 cells normalised to GAPDH. * $p < 0.05$,
258 ** $p < 0.01$, *** $p < 0.001$. n = 3 independent experiments.
259

260 **Alectinib and indisulam exacerbate RNA splicing defects, increase R-loop formation and**
261 **DNA damage.**

262 Proteomic data from our previous study (15) showed that indisulam exposure leads to an increase
263 in protein expression of most SRSF family members (**Supplementary Fig.4a**). Here, we observed
264 enhanced nuclear translocation of p-SRSF post-indisulam treatment, which was rescued in
265 *DCAF15*^{KO} cells (**Supplementary Fig.4b-c**), suggesting that SRPK1/SRSF pathway activation is
266 a compensatory mechanism following RBM39 degradation. RBM39 has previously been
267 identified as a potential SRPK1 target [25] and we observed a direct interaction between RBM39
268 and SRPK1 in neuroblastoma cells via Proximity Ligation Assay (PLA) (**Supplementary Fig.4d**).
269 This supports our hypothesis that the synergy between alectinib and indisulam arises from their

270 combined disruption of RNA splicing, by dually targeting interdependent spliceosomal
271 components, thereby limiting cellular adaptation.
272
273 To evaluate the impact of treatment on alternative splicing, IMR32 cells were treated with
274 alectinib, indisulam, or both for 24 hours. RNA-seq and rMATS analysis revealed that while
275 indisulam induced widespread splicing changes, particularly skipped exons (SE) and that alectinib
276 alone had a milder effect, combination treatment resulted in additional 7,646 altered events (33%)
277 and 1,758 mis-spliced genes (25%) beyond an additive effect (**Fig. 5a)**. Notably, alectinib-affected
278 genes largely overlapped with indisulam targets **(Fig. 5b)**, further supporting the likelihood of
279 functional cooperation between RBM39 and SRPK1. Gene ontology (GO) analysis of alternatively
280 spliced genes revealed enrichment in pathways regulating genome stability, including *DNA repair*,
281 *chromatin remodeling* and *DNA damage response* (**Fig. 5c)**. The significantly affected AS events
282 were plotted following combination treatment. (**Fig. 5d)**. Several most affected events were
283 validated through custom PCR primer design of affected exon regions (**Fig. 5e-f)**, confirming that
284 splicing disruption was significantly enhanced when combining RBM39 degraders and SRPK1
285 inhibition in both KELLY and IMR32 cells (**Fig. 5e-f, Supplementary Fig.5a**); such an effect was
286 not observed with lorlatinib or siALK (**Supplementary Fig.5b-d**). These results suggest the
287 synergy observed between alectinib and indisulam may be attributed to the compound reduction
288 of canonical isoform expression and enhanced functional loss in effected pathways, such as DNA
289 damage repair. For example, expression of the canonical CHK1 isoform was nearly abolished by
290 the co-treatment of indisulam with either alectinib or SPHINX31. Moreover, CHK1 protein was
291 depleted following indisulam and alectinib combination treatment (**Supplementary Fig.5e**),

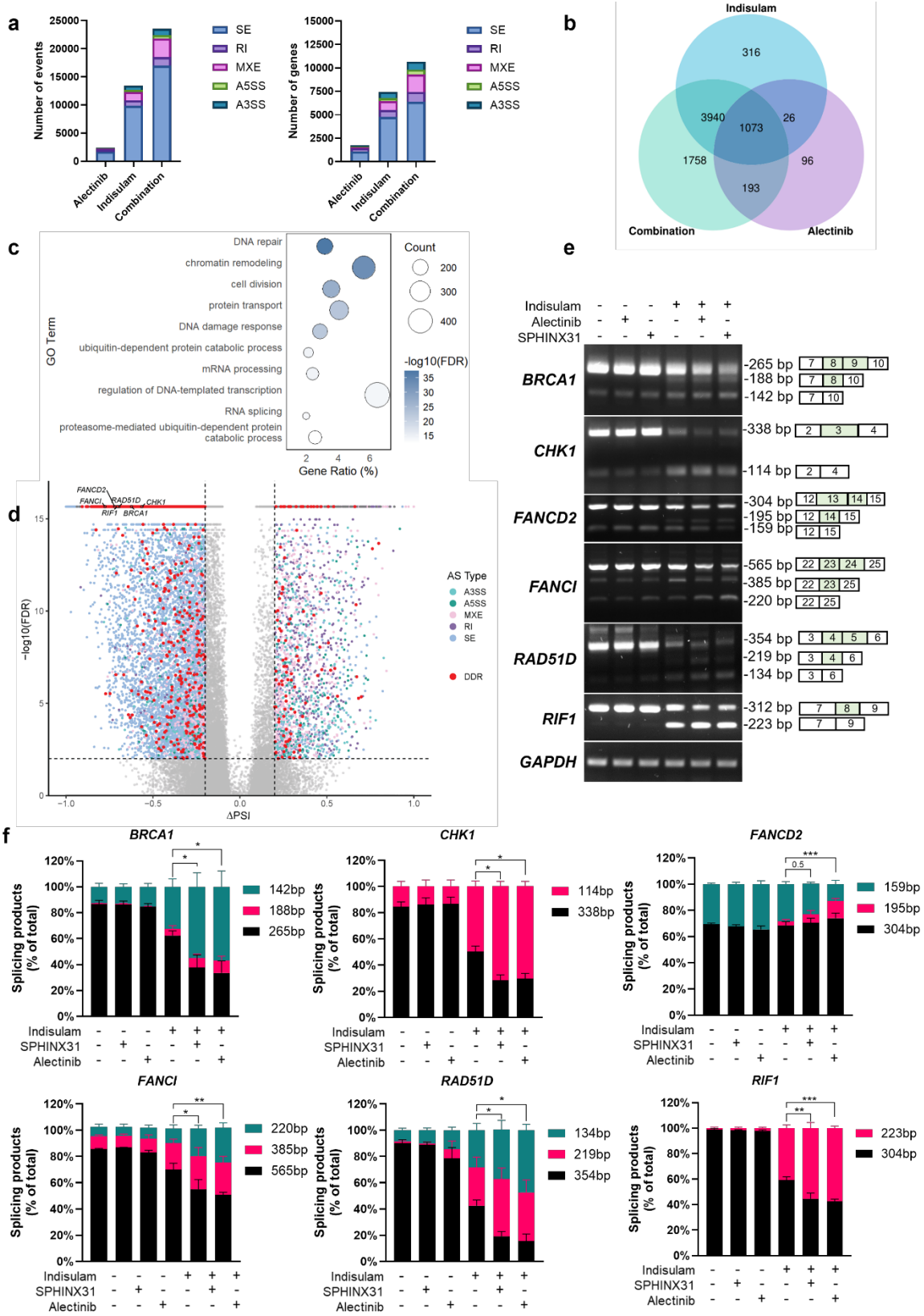
a
Number of events
Number of genes
SE
RI
MXE
A5SS
A3SS
Alectinib
Indisulam
Combination
b
Indisulam
Alectinib
Combination
316
3940
26
1073
1758
96
193
c
GO Term
DNA repair
chromatin remodeling
cell division
protein transport
DNA damage response
ubiquitin-dependent protein catabolic process
mRNA processing
regulation of DNA-templated transcription
RNA splicing
proteasome-mediated ubiquitin-dependent protein catabolic process
Gene Ratio (%)
Count
-log10(FDR)
d
FANCD2
FANCI
RAD51D
CHK1
RIF1
BRCA1
-log10(FDR)
ΔPSI
AS Type
A3SS
A5SS
MXE
RI
SE
DDR
e
Indisulam
Alectinib
SPHINX31
BRCA1
-265 bp
-188 bp
-142 bp
CHK1
-338 bp
-114 bp
FANCD2
-304 bp
-195 bp
-159 bp
FANCI
-565 bp
-385 bp
-220 bp
RAD51D
-354 bp
-219 bp
-134 bp
RIF1
-312 bp
-223 bp
GAPDH
f
BRCA1
142bp
188bp
265bp
CHK1
114bp
338bp
FANCD2
159bp
195bp
304bp
FANCI
220bp
385bp
565bp
RAD51D
134bp
219bp
354bp
RIF1
223bp
304bp
Splicing products (% of total)
Indisulam
SPHINX31
Alectinib

292

293 **Figure 5. Alternative-splicing elicited in neuroblastoma cells by treatment with alectinib,**
294 **indisulam and the combination. a** Number of alternative splicing (AS) events (left) and affected
295 genes (right) detected by rMATS, classified into exon skipping (SE), retained introns (RI),
296 mutually exclusive exons (MXE), alternative 5′ splice sites (A5SS), and alternative 3′ splice sites
297 (A3SS). **b** Venn diagram showing overlap of alternatively spliced genes across treatments. **c** Gene
298 Ontology (GO) enrichment analysis of AS genes in the combination group; dot size reflects gene
299 count, colour indicates –logFDR. **d** Volcano plots display $-\log_{10}$(FDR) values calculated by
300 rMATS. Events with FDR = 0, due to numerical underflow from highly significant p-values, were
301 assigned a nominal value of 1e–16 for visualisation purposes. Significant splicing events were
302 defined as those with FDR < 0.01 and $|\Delta \mathrm{PSI}| \geqslant 0.2$. DDR related genes are highlighted in red,
303 and six of these genes were selected for further experimental validation (labelled). **e** PCR
304 validation of exon skipping events in DDR genes (representative image of n=3). *GAPDH* was
305 included as a control. **f** Densitometry analysis of alternative splicing products, Two-way ANOVA
306 was used to detect the significance.
307
308 To determine whether splicing-induced depletion of DDR genes increased DNA damage, we
309 assessed γH2AX levels as a marker for DNA double stranded breaks(30). Immunofluorescence
310 and western blot showed significant γH2AX accumulation following combination treatment
311 compared to monotherapies (**Fig. 6a-b, Supplementary Fig.6a**). Importantly, this increase was
312 absent when indisulam was combined with lorlatinib (**Supplementary Fig.6b-c**), indicating that
313 the effect stems from RNA splicing disruption rather than ALK inhibition.
314

315 R-loops are DNA:RNA hybrids that are a product of intermediate transcription and must be
316 resolved to permit progression of replication forks (31,32). R-loop accumulation results in
317 transcription-replication collisions, which generate replication stress and double-strand breaks
318 (33). Many R-loop regulatory genes were mis-spliced after combination treatment. For example,
319 BRCA1 interacts with the putative RNA helicase Senataxin (SETX), forming a complex that
320 localizes to R-loops(34) and Fanconi Anemia genes recruit RNA processing enzymes to resolve
321 R-loops generated by moderate replication stress(35), while RIF1 facilitates replication fork
322 protection and efficient restart to maintain genome stability(36). Notably, SR proteins regulated
323 by SRPK1 can also impede R-loop formation(31). Dysregulation of these functions lead to
324 accumulation of unresolved R-loops, replication fork breakage, and genome instability (31).
325
326 We quantitated R-loops using S9.6 antibody(37). Treatment with either alectinib or SPHINX31
327 led to increased nuclear S9.6 staining indicating the accumulation of R-loops. The combination
328 treatment significantly increased R-loop formation as compared to monotherapies (**Fig. 6c-d,**
329 **Supplementary Fig.6d-f**). To evaluate replication stress induced by Rloop accumulation(31,38),
330 we quantified the intensity of phosphorylated RPA32 serine 33 (pRPA), a marker of single-
331 stranded DNA (ssDNA) at stalled replication forks. We observed an increase following exposure
332 to the combination treatment relative as compared to monotherapy (**Fig. 6e, Supplementary**
333 **Fig.6e**). DNA fibre analysis using BrdU and IdU labelling further revealed a reduction in track
334 length and the significantly decreased IdU/BrdU ratio following combination treatment, indicating
335 increased fork stalling and replication stress. Collectively, these findings suggest that dual
336 targeting of SRPK1 and RBM39 leads to the accumulation of unresolved R-loops, promoting
337 replication stress, and contributing to subsequent DNA damage in high-risk neuroblastoma.

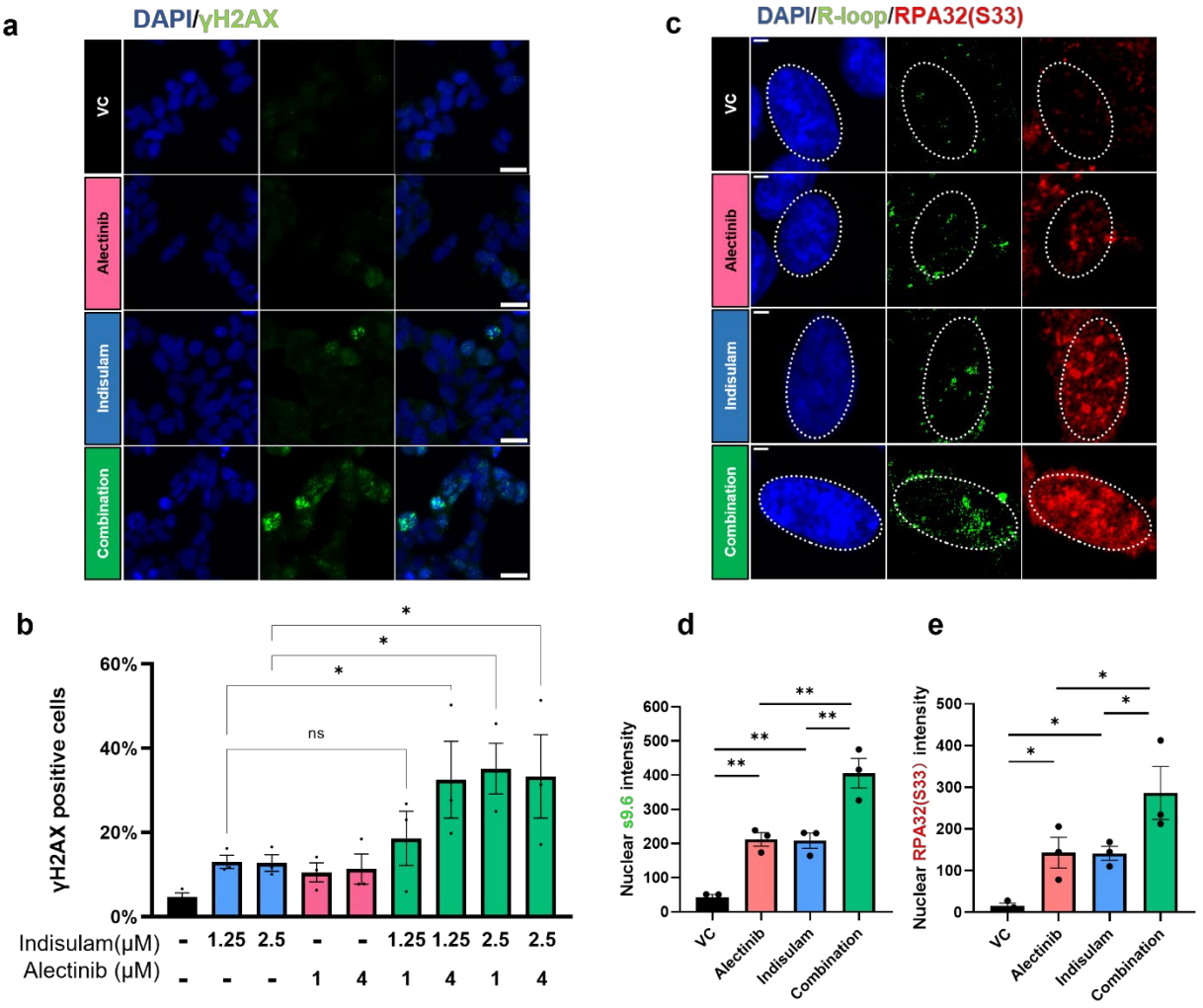

Figure 6. Combination of indisulam and alectinib induce DNA damage, R-loop accumulation and replication stress. A-b Immunofluorescence staining of γH2AX in KELLY cells treated with indisulam in combination of alectinib. Representative images of KELLY treated with 4μM alectinib and 1.25μM indisulam are shown. Scale bars = 20μm. Nuclear foci >5 indicates positive cells. n=3 independent experiments. **c** Representative images for nuclear S9.6 and RPA32 (S33) foci in KELLY cells, n = 3 independent experiments, Scale bars = 2.5μm. **d-e** Quantification of nuclear S9.6 intensity d and pRPA32 e intensity in KELLY cells. Cells were treated with 4μM alectinib monotherapy or with 1.25μM indisulam; nuclear signal intensity were measured by

347 merging to DAPI; n>300 cells from 3 independent experiments were quantified. Significance was
348 analysed among the median values.
349
350 **Combination of indisulam and alectinib improves survival in a Th-MYCN/ALK^{F1174L}**
351 **neuroblastoma model**
352 Gain-of-function mutations in ALK account for 10-15% of high-risk neuroblastoma (6). ALK
353 inhibitors have been shown to be safe and effective in treating ALK-driven neuroblastoma in a
354 Phase I trial(39,40), and are currently being investigated in several Phase III trials(39,41,42),
355 highlighting their potential for clinical use in ALK-positive neuroblastoma. Considering the clinic
356 relevance and benefit, we used an allograft mouse model implanted with Th-MYCN/ALK^{F1174L}
357 tumour cells derived from genetically engineered mouse models (GEMMs) (**Fig. 7a**).
358
359 Tumour-bearing mice were treated (indisulam 10mg/kg, alectinib 40mg/kg or combination) for 2-
360 weeks with a 45-day follow-up. Both monotherapies significantly enhanced survival however all
361 alectinib treated mice relapsed on treatment and 5/8 mice in the indisulam monotherapy group
362 relapsed after withdrawal of treatment. Complete tumour regression without subsequent relapses
363 resulting in a 100% survival rate were reported in the combination group (**Fig. 7b-c**) consistent
364 with the increased efficacy in-vitro.
365 Tumour samples were collected for pharmacodynamic analysis after 3 days of treatment. Western
366 blotting showed a clear depletion of RBM39 following indisulam and combination therapy,
367 confirming the on-target effect of indisulam (**Fig. 7d**). Furthermore, treatment with 10 mg/kg
368 indisulam reduced MYCN expression, as previously reported by Singh et al (43), suggesting a
369 potential link between RBM39 inhibition and suppression of MYCN (**Fig. 7d**). Additionally, a

370 decrease in p-ALK **(Supplementary Fig.7a)**, and a reduction in p-SRSF (**Fig. 7f**) confirmed the
371 on-target effects of alectinib on SRPK1 and ALK. Double strand breaks measured by accumulation
372 of γH2AX foci, were increased in combination therapies (**Fig. 7g**), in line with our observations
373 *in-vitro.* However, indisulam alone did not significantly induce γH2AX accumulation, possibly
374 due to the transient nature of γH2AX focus formation during the DNA damage response. However,
375 clear nuclear fragmentation was observed in mice treated with indisulam and combination therapy
376 (**Fig. 7g**). Importantly, no significant weight loss was observed during the trial, indicating no
377 significant toxicity (**Supplementary Fig.7b)**, and we observed no significant RBM39 loss in other
378 organs after 3-day treatment (**Supplementary Fig.7c**).
379 Taken together, these data confirm that in neuroblastoma the therapeutic benefit of RBM39-
380 depleting agents can be enhanced through combination with SRPK1 inhibitors, such as alectinib.
381 This study provides proof-of concept for the co-targeting of functionally interdependent splicing
382 factors using repurposed clinical agents to more effectively target aggressive childhood cancers
383 such as neuroblastoma. The strategy could apply more widely to other oncogene-driven cancers
384 that exhibit a high dependency on faithful splicing of mRNA.

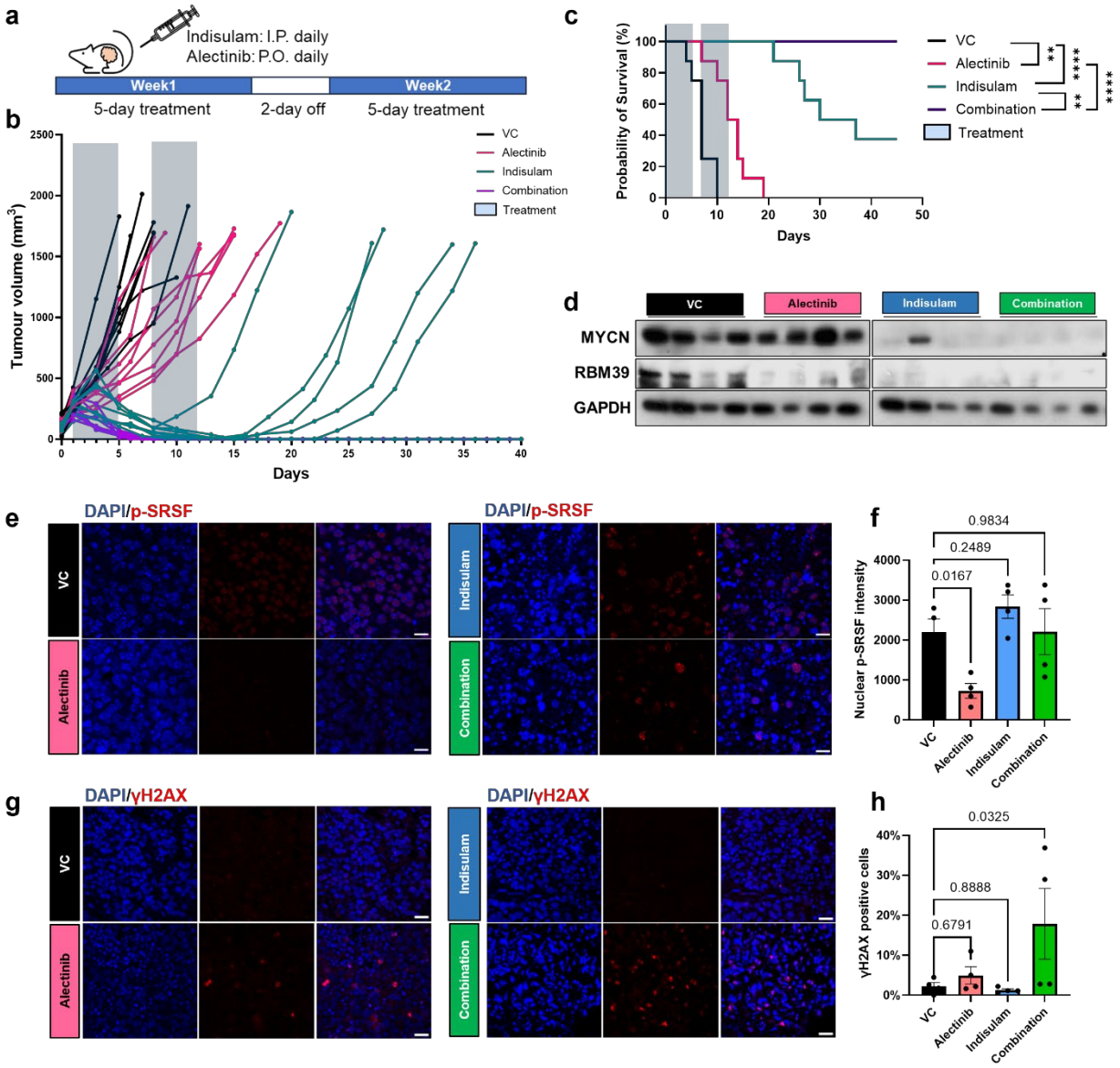

Figure 7. Combination of indisulam and alectinib suppress neuroblastoma tumour growth. **a** Th-ALK^{F1174L}/Th-MYCN GEMM tumour cells were injected into a cohort of mice subcutaneously, intravenous (i.v.) administration of 10 mg/kg of indisulam and oral gavage (p.o.) 40 mg/kg of alectinib for 2 weeks with 5 days on and 2 days off. **b** Tumour volume measured 3 times a week until the humane end-point was reached. Cyan shade indicates the treatment period. n = 8 for each group. **c** Survival plot of mice bearing Th-ALK^{F1174L}/Th-MYCN allografts treated

392 with vehicle or alectinib or indisulam or combination therapy. **d** Western blotting in tumour tissues
393 after administration of vehicle or alectinib or indisulam or combination therapy for 3 days (n = 4
394 per group). **e-h** Immunofluorescence staining was performed on tumour sections, with DAPI used
395 for nuclear staining. Nuclear p-SRSF intensity (E-F) was measured by merging to DAPI. Nuclear
396 γH2AX (G-H) foci >5 indicates positive cells. Scale bar = 20 μm. n.s. not significant, * $p < 0.05$,
397 **$p<0.01$, ***$p < 0.001$, ****$p < 0.0001$.
398

399 **DISCUSSION**

400 Indisulam has been recently identified as a molecular glue capable of regulating RNA alternative
401 splicing(2). By inducing splicing errors of genes in key oncogenic pathways, indisulam and other
402 spliceosomal inhibitors may render cancer cells susceptible to additional disruptions caused by
403 other anticancer drugs. Thus, it holds potential for implementation as combination therapy. We
404 performed extensive drug screens with FDA-approved anticancer agents which revealed several
405 potential drug-drug interactions with indisulam. Notably, the synergy between indisulam and
406 PARP inhibitors, also observed in our screens, has been corroborated by other studies in high-
407 grade ovarian carcinoma(18,20), colorectal cancer, and breast cancer(44), giving confidence in our
408 screening approach. Our study also highlights the fact that such screens can reveal beneficial
409 interactions based on polypharmacology(engagement of targets beyond the primary focus of
410 clinical development)(45), presenting novel rationales for drug repurposing.
411

412 High-risk neuroblastoma, which constitutes about 15% of all neuroblastoma cases, is characterized
413 by aggressive behaviour and poor prognosis(7). Gain-of-function mutations in ALK account for
414 10-15% of primary tumours (6), hence a number of trials have investigated the use of alectinib and

415 other ALK inhibitors in this clinical setting. While the more selective ALK inhibitor loratinib has
416 shown greater traction for the treatment of mutant ALK-driven neuroblastoma(39), treatment
417 resistance remains a significant clinical challenge(46). Our study demonstrates that the activity of
418 alectinib against SRPK1 can be exploited therapeutically in combination with other spliceosomal
419 inhibitors. This presents an interesting strategy to treat patients with emerging resistance to ALK
420 inhibitor therapy, including in lung cancer where alectinib has demonstrated much greater clinical
421 use(41) and beyond into other cohorts irrespective of ALK status. While other inhibitors of SRPKs
422 and related SRSF regulators such as Cirtuvivint(47) and TG-003(48) are currently in early
423 development, the fact that an established therapeutic tool can be repurposed in this way could
424 accelerate the clinical testing of SRPK1/2 inhibition and co-targeting of splicing factors as an anti-
425 cancer treatment strategy, particularly in tumours where an ALK inhibitor might normally be
426 indicated.
427
428 While we have successfully demonstrated the principle of co-targeting functionally interdependent
429 splicing as an anticancer strategy, several resulting questions arise. Our investigation into the
430 functional consequences of combined RBM39 degradation and SRPK1 inhibition underscores
431 their interdependency in regulating alternative splicing, but it is not yet clear if RBM39 is a direct
432 target of SPRK1 as has been suggested by global interaction profiling (49) and our co-localisation
433 experiments. More broadly, we need further investigation to understand the interactions and co-
434 regulation of different splicing factors that are also cancer targets such as RBM39 and SPRK1,
435 and to develop more detailed mechanistic models of how these regulate alternative splicing
436 together.
437

438 Interestingly, RNA-seq analysis revealed dual targeting SRPK1 and RBM39 synergiscally
439 amplifies RNA splicing dysfunction and downstream cellular stress. Targeting functionally
440 connected nodes within the splicing machinery may therefore offer an effective strategy to
441 overcome cellular adaptation and enhance therapeutic efficacy in high-risk neuroblastoma.
442 However, as with the targeting of spliceosomal components in general, it is unclear if the sequelae
443 of accumulating R loops, cell cycle arrest, DNA damage and eventual cell death that we observe
444 in combined SRPK1/RBM39 interference are lineage-dependent, driven by the mis-splicing and
445 functional loss of a select set of critical genes, or the cumulative consequence of widespread
446 alternative splicing events across multiple functional pathways. Further work to resolve such
447 mechanistic questions will be important to understand what the most relevant pharmacodynamic
448 readouts will be for future discovery experiments and which predictive biomarkers can best
449 identify patients most likely to benefit from such combinations (i.e. for stratification).
450
451 In summary, the present study supports a model in which co-treatment indisulam and alectinib
452 synergistically impacts RNA splicing through simultaneous RBM39 degradation and SRPK1
453 inhibition. This dual RNA splicing interference exacerbates splicing errors in key genes regulating
454 genome stability, leading to R-loop accumulation and increased DNA damage. These events
455 eventually result in cellular apoptosis and growth inhibition in high-risk neuroblastoma *in vitro*,
456 as well as suppression of tumour growth *in vivo*. These insights shed new light on translating
457 research on spliceosome inhibition into clinical applications, ultimately aiming to improve the
458 prognosis for patients with high-risk neuroblastoma.
459
460 **MATERIALS AND METHODS**

461 **Cell lines and cell culture**

462 Human neuroblastoma cell lines were cultured in MEM (Gibco™) with 10% fetal bovine serum
463 (FBS), 1% penicillin/streptomycin (P/S), 1 mM sodium pyruvate, and 2 mM L-glutamine.
464 KURAMOCHI was maintained in DMEM with 10% FBS, 2 mM L-glutamine, 5.6 mM glucose,
465 and 1% P/S. HCT116 was cultured in RPMI 1640 with 10% FBS, 2 mM L-glutamine, and 1% P/S.
466 All cells were authenticated and routinely tested for mycoplasma. Cells were maintained at 37°C
467 with 5% CO_2.

468 **Sulforhodamine B (SRB) assay**

469 Cells were fixed with 10% cold trichloroacetic acid, stained with 0.4% SRB for 30 min, and
470 washed with 1% acetic acid. Bound dye was solubilized in 10 mM Tris-base, and OD measured at
471 565 nm. Results were normalized to vehicle control.

472 **Synergy analysis**

473 Cell growth inhibition was assessed by SRB assay after 72 hours of drug exposure. The Loewe
474 additivity model was used to describe the interaction between two agents[32]. Synergy scores were
475 calculated using SynergyFinder web application (RRID:SCR_026127) to compute synergy scores
476 and the Loewe model was selected. Scores >10 indicate synergy, −10 to 10 additivity, and <−10
477 antagonism.

478 **siRNA Transfection**

479 Cells were seeded in 96-well plates and cultured overnight before transfection. ON-TARGETplus
480 Non-targeting Control Pool (Horizon Discovery, D-001810-10-05) and ON-TARGETplus siALK
481 (Horizon Discovery, L-003103-00-0005) (30 nM final concentration) were delivered using
482 Lipofectamine® 2000 (Invitrogen, 11668-019) in Opti-MEM (Gibco), following the

483 manufacturer's instructions. Opti-MEM only and Lipofectamine-only conditions were included as
484 controls. Cells were incubated for 16 h prior to further treatment..

485 **Western blotting**

486 Whole-cell lysates were prepared using RIPA buffer (Sigma Aldrich) with 1% HALT protease and
487 phosphatase inhibitor cocktail (Thermo Scientific). Equal amounts of protein from each sample
488 were separated on a 4-20% Bis-Tris SurePAGE gel (GenScript) and then transferred onto PVDF
489 membranes. The membranes were blocked with 5% milk for 1 hour at room temperature, followed
490 by an overnight incubation at 4°C with CHK1 (Cell Signaling Technology Cat# 2360,
491 RRID:AB_2080320), p-CHK1 (Cell Signaling Technology Cat# 2348, RRID:AB_331212),
492 γH2AX (Sigma-Aldrich Cat# 05-636, RRID:AB_309864). HRP-conjugated secondaries and
493 chemiluminescent substrate were used for detection.

494 **End-point and quantification PCR reactions**

495 1500ng RNA was utilized for reverse transcription. The resulting cDNA templates were
496 subsequently employed for qPCR using thePowerTrack SYBR Green Master Mix (Applied
497 Biosystems) or End-point PCR utilizing the Q5® High-Fidelity PCR Kit (New England Biolab).
498 PCR products were resolved on 2% agarose gels and quantified with Fiji V2.0.0.

Target genes	Primer (5' to 3')	Tm
BRCA1	AACTCTGAGGACAAAGCAGC CTTCTCAGTGGTGTTCAAATC	62
CHK1	GTGGAAGACTGGGACTTGGT ACCCCTGCCATGAGTTGATG	68
FANCD2	CGGTTACAGGCTTCCCAAGT GCTGTTCTTGAATGCAGCCT	67

FANCI	GAGTCAGGCCGAGAAGGTTC CAACGGCAGCAGGTTTCTC	68
RAD51D	TGGCTCAGTTCTCGGCTTT AGATGTCAAATGCATGCACCA	66
TP53BP1	GCTGTTGCTGAGTCTGTTGC TGCGTACTTCCCGGATTGTT	68
RIF1	AGGTGGGCAAAACTGGTCAT TGGGTGCTCCACTACGAAAT	67
VEGF165b	AAGAAAATCCCTGTGGGCCTT TGGTGAGAGATCTGCAAGTACGTT	60
VEGF165	AGAGCAAGACAAGAAAATCC TACAAACAAATGCTTTCTCC	53
GAPDH	GGCTGCTTTTAACTCTGG GGAGGGATCTCGCTCC	62

499 **Immunofluorescence staining**

500 KELLY cells were fixed with 4% PFA, permeabilized with 0.1% Triton-X100, and blocked in 5%
501 BSA. Subsequently, they were incubated overnight at 4°C with anti-phosphoepitope SR proteins
502 antibody (1:100, Millipore Cat# MABE50, RRID:AB_10807429) or γH2AX (1:500, Sigma-
503 Aldrich Cat# 05-636, RRID:AB_309864) in blocking buffer ,and then stained with a mix of Alexa
504 Fluor 488-conjugated goat anti-mouse antibody (1:500, AF488, Thermo Scientific), DAPI
505 (1µg/ml, Biotium, Cat#40043), and Phalloidin-647 (1:50, Cell Signaling Technology Cat#
506 #8940S) for 1 hour at room temperature. The cells were washed again three times with PBS-T
507 before imaging with an INCell Analyzer 1000 microscope (GE Healthcare) at 20x magnification.

508 S9.6 (1:250, Millipore Cat# MABE1095, RRID:AB_2861387) and phospho RPA32-S33 (1:250,
509 Novus Cat# NB100-544, RRID:AB_10002227) were detected in KELLY cells fixed with cold
510 methanol at -20°C for 10 minutes and slides were imaged using the Aurox laser-free confocal

511 microscope. To confirm the specificity of the S9.6 antibody, RNase H (Ribonuclease H, 1:100,
512 NEB Cat#M0297S) was applied to the fixed cells before antibody incubation.

513 Image analysis was performed using Cell Profiler V4.2.6, with nuclear regions masked by DAPI
514 staining and cytoplasmic regions masked by Phalloidin staining, excluding areas overlapping with
515 DAPI.

516 **SRPK1/2 kinase activity assay**

517 The SRPK1 Kinase Enzyme System (#VA7558, Promega) and SRPK2 Kinase Enzyme System
518 (#VA7561, Promega) were utilised with the ADP-Glo™ Kinase Assay (#V6930, Promega),
519 following the manufacturer's protocol. Briefly, 1 µl of inhibitor, diluted in 1X kinase reaction
520 buffer, was added to the wells of a 384-well low-volume plate and combined with 8 ng of SRPK1
521 enzyme. Following this, 2 µl of a substrate/ATP mixture (100 µM ATP, 0.1 µg/µl MBP) was
522 added. The reaction was incubated at room temperature for 1 hour. After incubation, 5 µl of ADP-
523 Glo™ Reagent was added to each well, and the plate was incubated at room temperature for 40
524 minutes. Subsequently, 10 µl of Kinase Detection Reagent was added, and the plate was incubated
525 for an additional 30 minutes. Luminescence was recorded.

526 **Proximity Ligation Assay (PLA)**

527 The Duolink® Proximity Ligation Assay (PLA) was used to detect protein-protein interactions in
528 KELLY cells. Samples were fixed with 4% paraformaldehyde, permeabilised with 0.1% Triton X-
529 100, and blocked with the Duolink® blocking solution. Primary antibodies against RBM39 (1:500,
530 Proteintech Cat# 67420-1-Ig, RRID:AB_2882660) and SRPK1 (1:250, Abcam Cat# ab90527,
531 RRID:AB_2050339) were applied overnight at 4°C. Species-specific PLA probes (Sigma-Aldrich)

532 were added, followed by ligation and rolling-circle amplification according to the manufacturer's
533 instructions.

534 **DNA fibre analysis**

535 Cells were sequentially pulse-labeled with 10 μM BrdU and 200 mM IdU for 30 minutes each.
536 KELLY cells were spotted on SuperFrost slides, air-dried for 5 minutes, and lysed with a buffer
537 (200 mM Tris-HCl, pH 7.5, 50 mM EDTA, 0.5% SDS) to release DNA and fixed in 75%
538 methanol/25% acetic acid, and then treated with 2.5M HCl for 1 hour to denature the DNA. After
539 blocking with 1% BSA in PBS-T for 1 hour. BrdU was detected by anti-BrdU antibody (1:50,
540 Abcam Cat# ab6326, RRID:AB_305426)) followed by AF647-conjugated secondary antibody
541 (1:100, A21247, Invitrogen). IdU was labeled with mouse anti-BrdU antibody (1:50, BD
542 Biosciences Cat# 347580, RRID:AB_10015219) and AF488-conjugated secondary antibody
543 (1:100, Thermo Fisher Scientific Cat# A-11001, RRID:AB_2534069). Slides were mounted and
544 imaged using a laser-free confocal microscope, with DNA track lengths measured in Fiji V2.0
545 (RRID:SCR_002285).

546 **In vivo allograft model of neuroblastoma**

547 Syngeneic tumours derived from TH-MYCN/ALK^{F1174L} genetically engineered mouse models
548 (GEMMs), were implanted into immune competent 129×1/SvJ mice. Group assignment was
549 random and treatment began when the implanted tumours reached a volume of over 200 mm³. The
550 dosing schedule continued for 2 weeks, with daily administration for 5 days followed by 2 days
551 off. Alectinib was dissolved in saline containing 40% PEG300, 10% DMSO, and 5% Tween, and
552 was administered orally at a dose of 10 μL/kg. Indisulam was dissolved in saline with 3.5% DMSO
553 and 6.5% Tween80 and was administered intravenously at a dose of 5 μL/kg. Tumour tissues were
554 excised two hours after the final dose of each compound. Half of the tumour was fixed in 4% PFA,

555 while the other half was snap-frozen for subsequent analysis. Investigators were blind for the
556 analysis of the study.

557 **Immunoassays on tissue samples**

558 Snap frozen tumours were lysed in 5% CHAPS buffer and western blotting was carried out for
559 RBM39 (Proteintech Cat# 67420-1-Ig, RRID:AB_2882660), ERK1/2 (Cell Signaling Technology
560 Cat# 4695, RRID:AB_390779), pERK1/2 (Cell Signaling Technology Cat# 9101,
561 RRID:AB_331646), phosphoepitope SR proteins (Millipore Cat# MABE50,
562 RRID:AB_10807429) and GAPDH (Cell Signaling Technology Cat# 2118, RRID:AB_561053).
563 ALK Meso Scale Discovery® immunoassays were performed as previously described(50)

564 **Immunofluorescence on tissue sections**

565 Tumours sections were deparaffinized and rehydrated using Xylene and a graded series of alcohol.
566 They were then boiled in 1% citric-acid buffer for 20 minutes and allowed to cool to room
567 temperature. The sections were blocked for 1 hour in TBS with 0.01% Triton (TBST) and 5%
568 BSA. Afterwards, γH2AX antibody (Cell Signaling Technology Cat# 9718, RRID:AB_2118009)
569 was applied at a 1:100 dilution overnight at 4°C. Alexa Fluor 568 goat anti-rabbit antibody
570 (1:1000) was incubated at room temperature for 1 hour. Images were captured using a confocal
571 microscope (LSM700, LSM T-PMT) and processed with ZEN2009 software (Black version,
572 Zeiss).

573 **RNA sequencing and alternative splicing analysis**

574 Total RNA was extracted and mRNA enriched using poly-T oligo-attached magnetic beads.
575 Strand-specific libraries were constructed and quantified by Qubit and Bioanalyzer and sequenced
576 on an Illumina NovaSeq 6000 platform using an S4 flow cell with 150 bp paired-end reads

577 (Novogene, Cambridge, UK). Sequencing reads were quality-filtered and clean reads were aligned
578 to the human reference genome (hg38) using HISAT2. Gene-level counts were generated using
579 featureCounts, and differential expression analysis was performed using DESeq2. Resulting p-
580 values were adjusted using the Benjamini-Hochberg method to control the false discovery rate
581 (FDR), with significance defined as adjusted p-value $\leqslant$ 0.05

582 Alternative splicing analysis was conducted using rMATS (v4.3.0), which detects five splice event
583 types: skipped exon (SE), mutually exclusive exon (MXE), alternative 5′ splice site (A5SS),
584 alternative 3′ splice site (A3SS), and retained intron (RI). Differential splicing events were
585 identified based on junction-spanning reads, with significance set at FDR < 0.05.

586 **Statistical Analysis**

587 Statistical analyses were conducted using GraphPad Prism 10. For normally distributed data, a
588 Student's t-test was applied to two-group comparisons; one-way or two-way ANOVA for three or
589 more groups. Specific tests are detailed in figure legends.

590

591 **Acknowledgments:** We are very grateful to the technicians from the Institute of Cancer
592 Research BSU animal center, Barbara Martins da Costa and Kevin Greenslade for supporting
593 animal work. We thank Prof. Matthew J Fuchter from Imperial College London and Dr Lizzie
594 Tucker from Institute of Cancer Research for providing helpful comments.

595 **Author contributions:**

596 Conceptualization: YM, AN, HCK

597 Methodology: YM, EP, YX, SQ, AN

598 Investigation: YM, EP, BMC, YX, CJ, SQ, NZ, LC, HCK, AN

599 Visualization: YM, YX, CJ, SQ, AN

600 Funding acquisition: LC, HCK, AN

601 Project administration: HCK, AN

602 Supervision: AN, HCK, LC,

603 Writing – original draft: YX, LC, HCK, AN

604 Writing – review & editing: all authors contributed to the review and editing of the paper.

605 **Conflict of interest disclosure statement:** Authors declare that they have no conflict of interest.

606 **Funding:** Imperial College London and China Scholarship Council joint PhD studentship
607 202208310101 (YM), 201808060050 (YX). AstraZeneca/NIHR Imperial BRC Imperial College
608 Research Fellowship (AN). Cancer Research UK Fellowship RCCCDF-Nov23/100003 (AN).
609 Cancer Research UK Discovery Programme Grant (A28278) (EP, BMC, LC); HEFCE/RAE
610 (LC). Ovarian Cancer Action (CW, AN). Cancer Research UK convergence Science Centre PhD
611 studentships SEBCATP-2024/100009 (NZ), CANCTA-2022\100007 (SQ).

612 **Data and materials availability:** The RNAseq data generated in this study have been deposited
613 in NCBI's Gene Expression Omnibus(51) under the accession number GSE299818.

614 **References**

615 1. Patel, A.A. and Steitz, J.A. (2003) Splicing double: insights from the second spliceosome. *Nat Rev Mol*
616 *Cell Biol*, **4**, 960-970.
617 2. Han, T., Goralski, M., Gaskill, N., Capota, E., Kim, J., Ting, T.C., Xie, Y., Williams, N.S. and Nijhawan,
618 D. (2017) Anticancer sulfonamides target splicing by inducing RBM39 degradation via recruitment to
619 DCAF15. *Science*, **356**.
620 3. Xu, C., Chen, X., Zhang, X., Zhao, D., Dou, Z., Xie, X., Li, H., Yang, H., Li, Q., Zhang, H. *et al.* (2021)
621 RNA-binding protein 39: a promising therapeutic target for cancer. *Cell Death Discov*, **7**, 214.
622 4. Uehara, T., Minoshima, Y., Sagane, K., Sugi, N.H., Mitsuhashi, K.O., Yamamoto, N., Kamiyama, H.,
623 Takahashi, K., Kotake, Y., Uesugi, M. *et al.* (2017) Selective degradation of splicing factor CAPERalpha
624 by anticancer sulfonamides. *Nat Chem Biol*, **13**, 675-680.
625 5. Bojko, J., Kollareddy, M., Szemes, M., Bellamy, J., Poon, E., Moukachar, A., Legge, D., Vincent, E.E.,
626 Jones, N., Malik, S. *et al.* (2024) Spliceosomal vulnerability of MYCN-amplified neuroblastoma is
627 contingent on PRMT5-mediated regulation of epitranscriptomic and metabolomic pathways. *Cancer Lett*,
628 **604**, 217263.
629 6. Matthay, K.K., Maris, J.M., Schleiermacher, G., Nakagawara, A., Mackall, C.L., Diller, L. and Weiss,
630 W.A. (2016) Neuroblastoma. *Nat Rev Dis Primers*, **2**, 16078.
631 7. Bechmann, N., Westermann, F. and Eisenhofer, G. (2023) HIF and MYC signaling in adrenal neoplasms of
632 the neural crest: implications for pediatrics. *Front Endocrinol (Lausanne)*, **14**, 1022192.
633 8. Otte, J., Dyberg, C., Pepich, A. and Johnsen, J.I. (2020) MYCN Function in Neuroblastoma Development.
634 *Front Oncol*, **10**, 624079.
635 9. Chen, Y., Takita, J., Choi, Y.L., Kato, M., Ohira, M., Sanada, M., Wang, L., Soda, M., Kikuchi, A.,
636 Igarashi, T. *et al.* (2008) Oncogenic mutations of ALK kinase in neuroblastoma. *Nature*, **455**, 971-974.
637 10. Shaw, A.T., Gandhi, L., Gadgeel, S., Riely, G.J., Cetnar, J., West, H., Camidge, D.R., Socinski, M.A.,
638 Chiappori, A., Mekhail, T. *et al.* (2016) Alectinib in ALK-positive, crizotinib-resistant, non-small-cell lung
639 cancer: a single-group, multicentre, phase 2 trial. *Lancet Oncol*, **17**, 234-242.
640 11. Alam, M.W., Borenas, M., Lind, D.E., Cervantes-Madrid, D., Umapathy, G., Palmer, R.H. and Hallberg, B.
641 (2019) Alectinib, an Anaplastic Lymphoma Kinase Inhibitor, Abolishes ALK Activity and Growth in
642 ALK-Positive Neuroblastoma Cells. *Front Oncol*, **9**, 579.
643 12. Lu, J., Guan, S., Zhao, Y., Yu, Y., Woodfield, S.E., Zhang, H., Yang, K.L., Bieerkehazhi, S., Qi, L., Li, X.
644 *et al.* (2017) The second-generation ALK inhibitor alectinib effectively induces apoptosis in human
645 neuroblastoma cells and inhibits tumor growth in a TH-MYCN transgenic neuroblastoma mouse model.
646 *Cancer Lett*, **400**, 61-68.
647 13. Zafar, A., Wang, W., Liu, G., Wang, X., Xian, W., McKeon, F., Foster, J., Zhou, J. and Zhang, R. (2021)
648 Molecular targeting therapies for neuroblastoma: Progress and challenges. *Med Res Rev*, **41**, 961-1021.
649 14. Houghton, P.J. and Kurmasheva, R.T. (2019) Challenges and Opportunities for Childhood Cancer Drug
650 Development. *Pharmacol Rev*, **71**, 671-697.
651 15. Nijhuis, A., Sikka, A., Yogev, O., Herendi, L., Balcells, C., Ma, Y., Poon, E., Eckold, C., Valbuena, G.N.,
652 Xu, Y. *et al.* (2022) Indisulam targets RNA splicing and metabolism to serve as a therapeutic strategy for
653 high-risk neuroblastoma. *Nat Commun*, **13**, 1380.
654 16. Singh, S., Quarni, W., Goralski, M., Wan, S., Jin, H., Van de Velde, L.A., Fang, J., Wu, Q., Abu-Zaid, A.,
655 Wang, T. *et al.* (2021) Targeting the spliceosome through RBM39 degradation results in exceptional
656 responses in high-risk neuroblastoma models. *Sci Adv*, **7**, eabj5405.
657 17. Anczukow, O. and Krainer, A.R. (2015) The spliceosome, a potential Achilles heel of MYC-driven tumors.
658 *Genome Med*, **7**, 107.
659 18. Xu, Y., Spear, S., Ma, Y., Lorentzen, M.P., Gruet, M., McKinney, F., Xu, Y., Wickremesinghe, C.,
660 Shepherd, M.R., McNeish, I. *et al.* (2023) Pharmacological depletion of RNA splicing factor RBM39 by
661 indisulam synergizes with PARP inhibitors in high-grade serous ovarian carcinoma. *Cell Rep*, **42**, 113307.
662 19. Hatcher, J.M., Wu, G., Zeng, C., Zhu, J., Meng, F., Patel, S., Wang, W., Ficarro, S.B., Leggett, A.L.,
663 Powell, C.E. *et al.* (2018) SRPKIN-1: A Covalent SRPK1/2 Inhibitor that Potently Converts VEGF from
664 Pro-angiogenic to Anti-angiogenic Isoform. *Cell Chem Biol*, **25**, 460-470 e466.
665 20. Xu, Y., Spear, S., Ma, Y., Lorentzen, M.P., Gruet, M., McKinney, F., Xu, Y., Wickremesinghe, C.,
666 Shepherd, M.R., McNeish, I. *et al.* (2023) Pharmacological depletion of RNA splicing factor RBM39 by

667 indisulam synergizes with PARP inhibitors in high-grade serous ovarian carcinoma. *bioRxiv*,
668 2023.2001.2018.524417.
669 21. BLISS, C.I. (1939) THE TOXICITY OF POISONS APPLIED JOINTLY1. *Annals of Applied Biology*, **26**,
670 585-615.
671 22. Uhlen, M., Bjorling, E., Agaton, C., Szigyarto, C.A., Amini, B., Andersen, E., Andersson, A.C., Angelidou,
672 P., Asplund, A., Asplund, C. *et al.* (2005) A human protein atlas for normal and cancer tissues based on
673 antibody proteomics. *Mol Cell Proteomics*, **4**, 1920-1932.
674 23. Infarinato, N.R., Park, J.H., Krytska, K., Ryles, H.T., Sano, R., Szigety, K.M., Li, Y., Zou, H.Y., Lee, N.V.,
675 Smeal, T. *et al.* (2016) The ALK/ROS1 Inhibitor PF-06463922 Overcomes Primary Resistance to
676 Crizotinib in ALK-Driven Neuroblastoma. *Cancer Discov*, **6**, 96-107.
677 24. Sakamoto, H., Tsukaguchi, T., Hiroshima, S., Kodama, T., Kobayashi, T., Fukami, T.A., Oikawa, N.,
678 Tsukuda, T., Ishii, N. and Aoki, Y. (2011) CH5424802, a selective ALK inhibitor capable of blocking the
679 resistant gatekeeper mutant. *Cancer Cell*, **19**, 679-690.
680 25. Tufail, M. and Wu, C. (2023) SRPKs: a promising therapeutic target in cancer. *Clin Exp Med*.
681 26. Nikas, I.P., Themistocleous, S.C., Paschou, S.A., Tsamis, K.I. and Ryu, H.S. (2019) Serine-Arginine
682 Protein Kinase 1 (SRPK1) as a Prognostic Factor and Potential Therapeutic Target in Cancer: Current
683 Evidence and Future Perspectives. *Cells*, **9**.
684 27. Pogacar, Z., Groot, K., Jochems, F., Dos Santos Dias, M., Mulero-Sanchez, A., Morris, B., Roosen, M.,
685 Wardak, L., De Conti, G., Velds, A. *et al.* (2022) Genetic and compound screens uncover factors
686 modulating cancer cell response to indisulam. *Life Sci Alliance*, **5**.
687 28. Batson, J., Toop, H.D., Redondo, C., Babaei-Jadidi, R., Chaikuad, A., Wearmouth, S.F., Gibbons, B.,
688 Allen, C., Tallant, C., Zhang, J. *et al.* (2017) Development of Potent, Selective SRPK1 Inhibitors as
689 Potential Topical Therapeutics for Neovascular Eye Disease. *ACS Chem Biol*, **12**, 825-832.
690 29. Amin, E.M., Oltean, S., Hua, J., Gammons, M.V.R., Hamdollah-Zadeh, M., Welsh, G.I., Cheung, M.K., Ni,
691 L., Kase, S., Renne, E.S. *et al.* (2011) WT1 Mutants Reveal SRPK1 to Be a Downstream Angiogenesis
692 Target by Altering VEGF Splicing. *Cancer Cell*, **20**, 768-780.
693 30. Burma, S., Chen, B.P., Murphy, M., Kurimasa, A. and Chen, D.J. (2001) ATM phosphorylates histone
694 H2AX in response to DNA double-strand breaks. *J Biol Chem*, **276**, 42462-42467.
695 31. Santos-Pereira, J.M. and Aguilera, A. (2015) R loops: new modulators of genome dynamics and function.
696 *Nat Rev Genet*, **16**, 583-597.
697 32. Hamperl, S. and Cimprich, K.A. (2016) Conflict Resolution in the Genome: How Transcription and
698 Replication Make It Work. *Cell*, **167**, 1455-1467.
699 33. Sridhara, S.C., Carvalho, S., Grosso, A.R., Gallego-Paez, L.M., Carmo-Fonseca, M. and de Almeida, S.F.
700 (2017) Transcription Dynamics Prevent RNA-Mediated Genomic Instability through SRPK2-Dependent
701 DDX23 Phosphorylation. *Cell Rep*, **18**, 334-343.
702 34. Hatchi, E., Skourti-Stathaki, K., Ventz, S., Pinello, L., Yen, A., Kamieniarz-Gdula, K., Dimitrov, S.,
703 Pathania, S., McKinney, K.M., Eaton, M.L. *et al.* (2015) BRCA1 recruitment to transcriptional pause sites
704 is required for R-loop-driven DNA damage repair. *Mol Cell*, **57**, 636-647.
705 35. Okamoto, Y., Abe, M., Itaya, A., Tomida, J., Ishiai, M., Takaori-Kondo, A., Taoka, M., Isobe, T. and
706 Takata, M. (2019) FANCD2 protects genome stability by recruiting RNA processing enzymes to resolve R-
707 loops during mild replication stress. *FEBS J*, **286**, 139-150.
708 36. Mukherjee, C., Tripathi, V., Manolika, E.M., Heijink, A.M., Ricci, G., Merzouk, S., de Boer, H.R.,
709 Demmers, J., van Vugt, M. and Ray Chaudhuri, A. (2019) RIF1 promotes replication fork protection and
710 efficient restart to maintain genome stability. *Nat Commun*, **10**, 3287.
711 37. Phillips, D.D., Garboczi, D.N., Singh, K., Hu, Z., Leppla, S.H. and Leysath, C.E. (2013) The sub-
712 nanomolar binding of DNA-RNA hybrids by the single-chain Fv fragment of antibody S9.6. *J Mol*
713 *Recognit*, **26**, 376-381.
714 38. Promonet, A., Padioleau, I., Liu, Y., Sanz, L., Biernacka, A., Schmitz, A.L., Skrzypczak, M., Sarrazin, A.,
715 Mettling, C., Rowicka, M. *et al.* (2020) Topoisomerase 1 prevents replication stress at R-loop-enriched
716 transcription termination sites. *Nat Commun*, **11**, 3940.
717 39. Goldsmith, K.C., Park, J.R., Kayser, K., Malvar, J., Chi, Y.Y., Groshen, S.G., Villablanca, J.G., Krytska,
718 K., Lai, L.M., Acharya, P.T. *et al.* (2023) Lorlatinib with or without chemotherapy in ALK-driven
719 refractory/relapsed neuroblastoma: phase 1 trial results. *Nat Med*, **29**, 1092-1102.
720 40. Suk, Y. and Singh, S.K. (2023) Safety and efficacy of lorlatinib against ALK-driven refractory or relapsed
721 neuroblastoma. *Cell Rep Med*, **4**, 101071.

722 41. Peters, S., Camidge, D.R., Shaw, A.T., Gadgeel, S., Ahn, J.S., Kim, D.W., Ou, S.I., Perol, M.,
723 Dziadziuszko, R., Rosell, R. *et al.* (2017) Alectinib versus Crizotinib in Untreated ALK-Positive Non-
724 Small-Cell Lung Cancer. *N Engl J Med*, **377**, 829-838.
725 42. Solomon, B.J., Liu, G., Felip, E., Mok, T.S.K., Soo, R.A., Mazieres, J., Shaw, A.T., de Marinis, F., Goto,
726 Y., Wu, Y.L. *et al.* (2024) Lorlatinib Versus Crizotinib in Patients With Advanced ALK-Positive Non-
727 Small Cell Lung Cancer: 5-Year Outcomes From the Phase III CROWN Study. *J Clin Oncol*, **42**, 3400-
728 3409.
729 43. Singh, S., Quarni, W., Goralski, M., Wan, S.B., Jin, H.J., Van de Velde, L.A., Fang, J., Wu, Q., Abu-Zaid,
730 A., Wang, T.T. *et al.* (2021) Targeting the spliceosome through RBM39 degradation results in exceptional
731 responses in high-risk neuroblastoma models. *Science Advances*, **7**.
732 44. Kohsaka, S., Yagishita, S., Shirai, Y., Matsuno, Y., Ueno, T., Kojima, S., Ikeuchi, H., Ikegami, M., Kitada,
733 R., Yoshioka, K.I. *et al.* (2024) A molecular glue RBM39-degrader induces synthetic lethality in cancer
734 cells with homologous recombination repair deficiency. *NPJ Precis Oncol*, **8**, 117.
735 45. Kabir, A. and Muth, A. (2022) Polypharmacology: The science of multi-targeting molecules. *Pharmacol*
736 *Res*, **176**, 106055.
737 46. Tucker, E.R., Jimenez, I., Chen, L., Bellini, A., Gorrini, C., Calton, E., Gao, Q., Che, H., Poon, E., Jamin,
738 Y. *et al.* (2023) Combination Therapies Targeting ALK-aberrant Neuroblastoma in Preclinical Models.
739 *Clin Cancer Res*, **29**, 1317-1331.
740 47. Tam, B.Y., Chiu, K., Chung, H., Bossard, C., Nguyen, J.D., Creger, E., Eastman, B.W., Mak, C.C., Ibanez,
741 M., Ghias, A. *et al.* (2020) The CLK inhibitor SM08502 induces anti-tumor activity and reduces Wnt
742 pathway gene expression in gastrointestinal cancer models. *Cancer Lett*, **473**, 186-197.
743 48. Sakuma, M., Iida, K. and Hagiwara, M. (2015) Deciphering targeting rules of splicing modulator
744 compounds: case of TG003. *Bmc Mol Biol*, **16**.
745 49. Buljan, M., Ciuffa, R., van Drogen, A., Vichalkovski, A., Mehnert, M., Rosenberger, G., Lee, S.,
746 Varjosalo, M., Pernas, L.E., Spegg, V. *et al.* (2020) Kinase Interaction Network Expands Functional and
747 Disease Roles of Human Kinases. *Mol Cell*, **79**, 504-520 e509.
748 50. Tucker, E.R., Tall, J.R., Danielson, L.S., Gowan, S., Jamin, Y., Robinson, S.P., Banerji, U. and Chesler, L.
749 (2017) Immunoassays for the quantification of ALK and phosphorylated ALK support the evaluation of on-
750 target ALK inhibitors in neuroblastoma. *Mol Oncol*, **11**, 996-1006.
751 51. Clough, E., Barrett, T., Wilhite, S.E., Ledoux, P., Evangelista, C., Kim, I.F., Tomashevsky, M., Marshall,
752 K.A., Phillippy, K.H., Sherman, P.M. *et al.* (2024) NCBI GEO: archive for gene expression and
753 epigenomics data sets: 23-year update. *Nucleic Acids Res*, **52**, D138-D144.
754

755